Eurasian Journal of Physics and Functional Materials

Volume 9 | Number 3

Article 2

Pages: 1 - 1

2025

Assessing the Influence of Level Density and Gamma Strength Function on Cross-Section and Isomeric Ratio in Bremsstrahlung-Induced Reaction of Tellurium Isotopes within GDR Region Using Talys 2.0 and Geant4

Bui Minh Hue
Institute of Physics, VAST, 10 Dao Tan St., Ba Dinh Dist., Hanoi, Vietnam, bmhue@iop.vast.vn

Tran Duc Thiep
Institute of Physics, VAST, 10 Dao Tan St., Ba Dinh Dist., Hanoi, Vietnam

Follow this and additional works at: https://www.ephys.kz/journal

Recommended Citation
Hue, Bui Minh and Thiep, Tran Duc (2025) "Assessing the Influence of Level Density and Gamma Strength Function on Cross-Section and Isomeric Ratio in Bremsstrahlung-Induced Reaction of Tellurium Isotopes within GDR Region Using Talys 2.0 and Geant4," *Eurasian Journal of Physics and Functional Materials*: Vol. 9: No. 3, Article 2.
DOI: https://doi.org/10.69912/2616-8537.1250

This Original Study is brought to you for free and open access by Eurasian Journal of Physics and Functional Materials. It has been accepted for inclusion in Eurasian Journal of Physics and Functional Materials by an authorized editor of Eurasian Journal of Physics and Functional Materials.

ORIGINAL STUDY

Assessing the Influence of Level Density and Gamma Strength Function on Cross-section and Isomeric Ratio in Bremsstrahlung-induced Reaction of Tellurium Isotopes Within GDR Region Using TALYS 2.0 and GEANT4

Bui Minh Hue*, Tran Duc Thiep

Institute of Physics, Vietnam Academy of Science and Technology, 10 Dao Tan, Giang Vo, Hanoi 10000, Viet Nam

Abstract

This work reports the theoretical calculations of cross-section and isomeric ratios (IR) of ^{119m,g}Te, ^{121m,g}Te, ^{127m,g}Te and ^{129m,g}Te generated through bremsstrahlung-induced photonuclear reactions on natural Te target in the Giant Dipole Resonance (GDR) region. The IRs were computed as a function of bremsstrahlung endpoint energies, varying from 10 to 25 MeV. This was accomplished by convolving differential cross-sections calculated by TALYS 2.0 code and bremsstrahlung spectra simulated by the GEANT4 toolkit. To assess the influence of nuclear level density (LD) and gamma strength functions (γSF) on cross-sections and IRs, we computed and evaluated all available LD and γSF models within TALYS 2.0 code, including 60 combinations. The outcomes were compared with experimental data from the EXFOR database, confirming the validity of the GEANT4 and TALYS codes as reliable tools for predicting cross-sections and IRs of Te isotopes in photonuclear reactions within the GDR region. Furthermore, the results highlight the significant role of LD models and γSFs in accurately modeling and estimating photonuclear reaction cross-sections and IRs.

Keywords: Isomeric ratio, Cross-section, Bremsstrahlung-induced reaction, GDR region, TALYS 2.0 code, GEANT4 toolkit

1. Introduction

Photonuclear reactions in the Giant Dipole Resonance (GDR) region, typically occurring within the photon energy range of 10−30 MeV, result from photon-induced collective nucleon excitation in the nucleus, characterized by a large photon absorption cross-section peak [1]. Understanding photonuclear reactions in the GDR region and the formation of isomeric states are crucial in the study of nuclear structure, reaction mechanism, applications, and stellar nucleosynthesis. The GDR region is particularly important in modeling the processes that occur during supernovae and other astrophysical events [2]. Owing to the scarcity of high-intensity quasi-monoenergetic photon sources, the majority of photonuclear data have been derived from bremsstrahlung-induced reactions. Bremsstrahlung spectra exhibit a continuous energy distribution, rendering the direct determination of differential cross-sections nearly impossible. Consequently, alternative approaches, such as measurements of yield, flux-weighted average cross-sections, integrated cross-sections, and isomeric yield ratio (IR), have been developed and utilized [3−11]. IR represents the relative population of an isomeric state versus an unstable ground state, garnering significant scientific interest in photonuclear reactions within the GDR region. It provides valuable insights into nuclear structure, properties, and reaction mechanisms, as it strongly correlates with various factors such as the

Received 23 December 2024; revised 18 June 2025; accepted 18 June 2025.
Available online 7 October 2025

* Corresponding author at: Institute of Physics, Vietnam Academy of Science and Technology, Hanoi 10000, Viet Nam.
E-mail address: bmhue@iop.vast.vn (B.M. Hue).

https://doi.org/10.69912/2616-8537.1250
2616-8537/© 2025 L.N. Gumilyov Eurasian National University. This is an open access article under the CC BY 4.0 DEED Attribution 4.0 International (https://creativecommons.org/licenses/by/4.0/).

energy and angular momentum of the incident projectile, LD, γSF, and the spin distribution of the excited nucleus [5−20]. Furthermore, the study of IR is essential for validating various nuclear reaction models. The experimental data on IRs for many nuclei remain scarce and incomplete, hindering a comprehensive understanding of their behavior. This underscores a significant need for theoretical predictions to supplement the gaps in experimental measurements, offering a more complete perspective on nuclear processes and improving model accuracy.

The initial theoretical calculations of IR were investigated and introduced by Huizenga and Vandebosch in the 1960s [13,14]. The Huizenga − Vandebosch model for IR calculation has limitations, particularly in assuming a constant spin cut-off parameter, which ignores its variation with excitation energy. The model's accuracy is further affected by assumptions regarding γ-ray cascade multiplicity and multipolarity, as well as the neglect of detailed nuclear level structure during final γ-cascade calculations. To date, numerous advanced computational codes have been developed and employed to calculate reaction cross-sections based on sophisticated nuclear models. Among the most prominent for simultaneously predicting nuclear reaction channels are GNASH [21], ALICE [22], STAPRE [23], EMPIRE [24], and TALYS [25,26]. TALYS is a robust and versatile computational code system for analyzing and forecasting nuclear reactions, enabling detailed simulations of reactions induced by *n, p, γ, d, t,* ^{3}He, and ^{4}He covering an energy range from 1 keV to 200 MeV. It employs the latest nuclear models and relies on validated nuclear structure parameters to calculate cross-sections, reaction rates, and other nuclear properties. Moreover, TALYS code is user-friendly, easy to use, frequently updated, and commonly employed alongside experimental data to produce reliable results for nuclear physics, astrophysics, medical isotope production, and nuclear reactor, offering greater flexibility and accessibility compared to many other codes.

The accuracy of statistical models for predicting compound nuclear reaction cross-sections is highly dependent on nuclear input models, particularly LD, γSF, and optical potentials. LD is a primary source of uncertainty, as it directly influences the probability of nuclear transitions or decays. Meanwhile, γSF is another essential input for determing photo-irradiated reaction cross-sections in the GDR region. To enhance predictive reliability, model calculations employing various combinations of LD and γSF are validated against experimental data, facilitating the identification of the most accurate inputs. The TALYS code [25−28] offers various options for LDs and γSFs, enabling the exploration of optimal combinations to minimize uncertainties in photonuclear reaction cross-sections. The calculation of IR requires not only the cross-sections computed using TALYS but also the bremsstrahlung spectral flux, which can be derived using Monte Carlo simulation frameworks like GEANT4 [29], MCNP [30], or FLUKA [31]. GEANT4 is a freely available, open-source software developed by CERN for simulating particle interactions with matter, providing capabilities for modeling particle tracking, detector geometry, and associated physical processes. One of the key advantages of GEANT4 is its flexibility, allowing users to build their simulation applications by extending predefined virtual classes.

Tellurium (Te) in its natural form comprises eight isotopes with the following isotope abundances: ^{120}Te (0.09 %), ^{122}Te (2.55 %), ^{123}Te (0.89 %), ^{124}Te (4.74 %), ^{125}Te (7.07 %), ^{126}Te (8.84 %), ^{128}Te (31.74 %), and ^{130}Te (34.08 %). The isotopes of Te and their isomeric states are of significant interest in nuclear structures, astrophysics, medical isotope production and nuclear reactor. Specifically, ^{120}Te, ^{122}Te, ^{123}Te, ^{124}Te, and ^{130}Te are used to produce iodine radioisotopes (^{120}I, ^{122}I, ^{123}I, ^{124}I and ^{131}I) for applications in PET imaging, gamma imaging, and thyroid diagnostics and thyroid cancer treament [32−34]. Moreover, ^{120}Te is one of the nuclei involved in the proton capture process (p-process), the process that mainly involves (γ, p), (γ, alpha) and (γ, n) reactions, which reaction rates are mostly calculated using Hauser-Feshbach statistical model [2]. Photonuclear reactions on heavier Te isotopes also play important roles in the slow neutron capture process (s-process). The (n, γ) reaction rates that are important for the s-process calculation can be constrained using the inverse (γ, n) cross-section. Te isotopes provide crucial insights into the development of IR as neutron subshell populations vary across a wide mass range (A = 119−130). With two protons above the Z = 50 shell closure and N = 67−79 neutrons, these isotopes are particularly valuable for testing nuclear models due to their small valence proton number and extensive valence neutron range, spanning from mid-shell to near the N = 82 closure.

There is limited research available on reaction cross-sections for Te isotopes in the (γ, n) reaction within the 10−25 MeV energy range. The EXFOR library [35] shows that only one publication exists for ^{120}Te [36], and one for ^{128}Te and ^{130}Te [37]. Studies on IR are slightly more extensive, with four publications on ^{119m,g}Te [10,16,18,20] and ^{121m,g}Te [10,16,19,20], three on ^{127m,g}Te [10,17,19], and seven on ^{129m,g}Te [10,15,17−20]. However, significant discrepancies remain among experimental results, and notably, no comprehensive theoretical study has been conducted to investigate the effects of different LD and γSF models

on the cross-sections and IRs of Te isotopes in the GDR region.

This study aims to evaluate the impact of various LD and γSF models on cross-section and IR calculations in (γ, n) reactions on ^{120}Te, ^{122}Te, ^{128}Te, and ^{130}Te nuclei at bremsstrahlung endpoint energies of 10−25 MeV, using the TALYS 2.0 code and GEANT4 toolkit and determine the most consistent LD and γSF model via comparisons with the experimental data.

2. Materials and methods

2.1. Calculation of cross-section using TALYS-2.0 code

The TALYS 2.0 code utilizes default keywords such as the projectile, target element, target mass, and projectile energy. With around 400 available keywords, TALYS 2.0 allows customization based on the user's objectives. In this study, beyond the default keywords, additional keywords associated with LD models and γSFs were used to compute the cross-sections. The LD and γSF models include both phenomenological approaches, derived from empirical parameterizations of nuclear properties, and microscopic models based on detailed quantum mechanical calculations. Phenomenological models generally rely on a set of free parameters, the values of which are determined through direct fitting to the limited experimental data. In contrast, the outputs of most microscopic models must be normalized to the available experimental data before being incorporated into statistical model calculations. It is important to emphasize that in this work, no normalization factor ($G_{norm} = 1$ in all calculations) is applied when comparing the results with experimental data.

The TALYS 2.0 code implements six level density (LD) models, consisting of three phenomenological models and three derived from microscopic calculations: Constant Temperature plus Fermi Gas Model (CT + FG) [**LD1**]: Merges the constant temperature model for low excitation energies with the Fermi gas model at higher energies; Back-shifted Fermi Gas Model (BSFG) [**LD2**]: Modifies the Fermi gas model by introducing an energy back-shift to improve agreement with experimental observations; Generalized Superfluid Model (GSM) [**LD3**]: A phenomenological model that incorporates nuclear pairing effects, essential for describing superfluid behavior in nuclei; Microscopic Level Density Models: These are derived from nuclear structure calculations using the Hartree-Fock-Bogoliubov framework and stored in tabulated form: Skyrme-Hartree-Fock-Bogolyubov level densities (SHFB) [**LD4**], Skyrme-Hartree-Fock-Bogolyubov combinatorial level densities (SHFBC) [**LD5**], Temperature-dependent Gogny-Hartree-Fock-Bogolyubov combinatorial level densities (TGHFBC) [**LD6**].

The TALYS 2.0 code includes ten models for the electric dipole (E1) γSF, each offering distinct approaches to modeling the E1 transition: Kopecky-Uhl Generalized Lorentzian (KUGL) [**S1**]: Commonly referred to as the generalized Lorentzian model (GLO), this approach, developed by Kopecky and Uhl, accounts for the energy and temperature dependence of the E1 transition width; Brink-Axel Lorentzian (BAL) [**S2**]: A standard Lorentzian model that complies with the Brink-Axel hypothesis; Hartree-Fock Bardeen-Cooper-Schrieffer (HF-BCS) [**S3**]: Utilizes the Hartree-Fock approach coupled with Bardeen-Cooper-Schrieffer (BCS) theory to generate level density tables; Hartree-Fock-Bogoliubov (HFB) [**S4**]: Based on the Hartree-Fock-Bogoliubov method for nuclear structure calculations; Goriely's Hybrid Model (GHM) [**S5**]: Combines microscopic HFB predictions for lower energies with a phenomenological GLO model for higher energies, particularly near the Giant Dipole Resonance (GDR); Goriely's Temperature-Dependent Hartree-Fock-Bogoliubov (GT-HFB) [**S6**]: Enhances the HFB framework by incorporating temperature dependence and QRPA corrections, as developed by Goriely; Temperature-Dependent Relativistic Mean Field (T-RMF) [**S7**]: A temperature-dependent relativistic mean field model proposed by Daoutidis and Goriely; Gogny D1M HFB + QRPA [**S8**]: Applies the HFB approach combined with QRPA, using the D1M version of the Gogny force, as calculated by Goriely; Simplified Modified Lorentzian Model (SMLO) [**S9**]: Offers a simplified variant of the traditional Lorentzian framework; Skyrme HFB + QRPA (S-HFB + QRPA) [**S10**]: Integrates the HFB model with QRPA, calculated using the Skyrme force, as developed by Goriely.

This study systematically examined the influence of various LD and γSF models on IRs by employing six LD models and ten γSF models, yielding 60 model combinations to compute cross-sections for photon-induced reactions on ^{nat}Te target. Calculations were performed across an energy range spanning from the (γ, n) reaction threshold to 25 MeV, with an increment of 0.1 MeV. All potential reaction exit channels corresponding to the specified projectile energy were included in the calculations.

2.2. Simulation of bremsstrahlung using GEANT4 toolkit

Bremsstrahlung production was simulated using Monte Carlo method in the GEANT4 toolkit, which accurately modeled the experimental setup in Refs. [10,15,19,20]. This includes modeling the detector geometry, materials, the primary beam, and accounting for all relevant interactions and radiation events.

Primary electron beams were generated using the G4GeneralParticleSource class, which allows flexible control over particle type, energy, and spatial and angular distributions via macro commands. The electron beam simulation used a circular profile and Gaussian energy distribution, matched to experimental conditions. The "Shielding" physics list, a pre-configured GEANT4 package developed at the SLAC, was selected for its accurate combination of electromagnetic and hadronic physics, including G4EmStandardPhysics and G4EmExtraPhysics, making it ideal for modeling γ-ray flux. The geometry of the setup was modeled in detail using custom implementations based on the virtual G4DetectorConstruction class. GEANT4 tracks individual particle histories, with the overall behavior reflecting cumulative effects across particles. Photon tracking was enabled following target modeling and source configuration, with detailed "delta" (δ) photon information extracted. Photon energy before target interaction was stored in a CERN ROOT [38] NTuples file, utilizing the user-defined G4UserSteppingAction class in GEANT4 for implementation. Analysis of the NTuples data revealed bremsstrahlung as a function of photon energy. The bremsstrahlung beam was produced through high-energy electron interactions with a primary tungsten (W) target (converter). Separate simulations were performed for bremsstrahlung spectra over endpoint energies from 10 to 25 MeV in 1 MeV steps.

2.3. Calculation of isomeric ratio

The theoretical IRs for bremsstrahlung-induced photonuclear reactions are computed by using the formula:

$$IR = \frac{N_0 \int_{E_{th}^m}^{E_\gamma^m} \sigma_m(E)\phi(E)dE}{N_0 \int_{E_{th}^g}^{E_\gamma^m} \sigma_g(E)\phi(E)dE}, \quad (1)$$

Here, N_0 represents the number of target nuclei, $E_{th}^{m(g)}$ denotes the threshold energy for the isomeric (ground) state, E_γ^m is the bremsstrahlung endpoint energy, $\sigma_{m(g)}(E)$ refers to the cross-section for the isomeric (ground) state, and ϕ(E) stands for the bremsstrahlung flux. The bremsstrahlung spectrum was simulated using GEANT4 and subsequently convolved with theoretical cross-sections calculated by the TALYS 2.0 code to derive theoretical IRs, as outlined in Formula (1).

3. Results and discussion

3.1. The bremsstrahlung spectra

The energy-dependent bremsstrahlung flux distribution was modeled using the GEANT4 toolkit. The simulation setup, including geometry, materials, and the primary electron beam, was designed to replicate the experimental conditions described in Refs. [10,15,19,20]. Fig. 1 illustrates the simulated bremsstrahlung spectra for endpoint energies ranging from 10 to 25 MeV, generated using the GEANT4 toolkit.

3.2. Cross-sections

The total cross-sections in the photonuclear reactions on ^{nat}Te within the GDR region were computed using

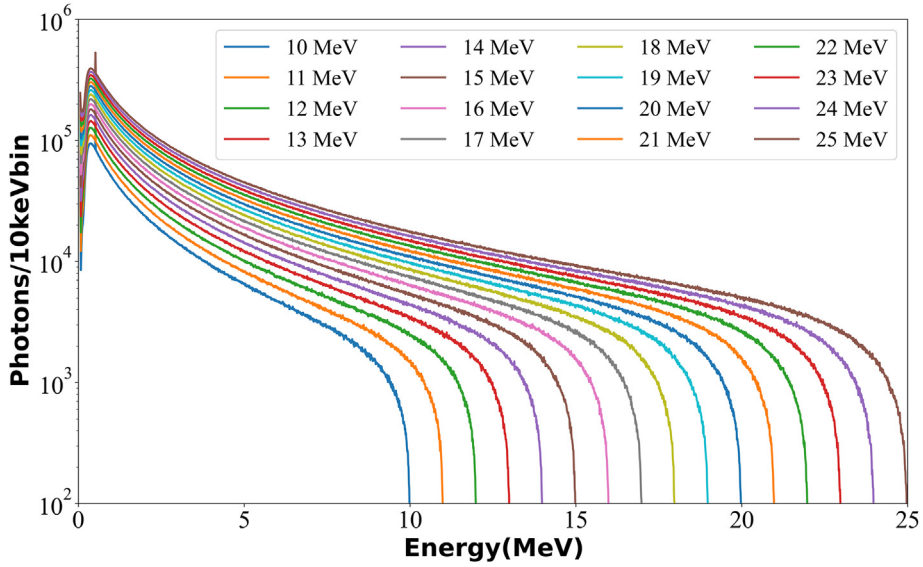

Fig. 1. The bremsstrahlung spectra generated employing the GEANT4 toolkit.

all possible mergers of LD and γSF in TALYS 2.0, and the outcomes are then validated by experimental values in EXFOR database [35]. Figs. 2−5 show the calculated cross-sections of ^{120,122,128,130}Te nuclei in the (γ, n) reactions compared with the experimental measurements in Refs. [36,37]. It is noted that only the experimental data taken from Ref. [36] are available for the ^{120}Te(γ, n)^{119}Te reaction. These data were obtained using a bremsstrahlung beam produced by the Microtron MT-30. The reaction cross-sections were not directly measured but inferred from yield measurements through the inverse matrix method. For reactions ^{128}Te(γ, n)^{127}Te and ^{130}Te(γ, n)^{129}Te, the measured experimental data in Ref. [37] using a quasi-monoenergetic photon beam produced at the 60 MeV LINAC at Saclay.

In the Fig. 2, the γSF theories can be seen showing two categories: the theories with one (KUGL [S1], BAL [S2], HFB [S4], GHM [S5], GT-HFB [S6], GD1M HFB + QRPA [S8] and SMLO [S9]) and two resonances (the rest including HF-BCS [S3], T-RMF [S7], S-HFB + QRPA [S10]), while the measured data illustrate only one peak. It should be noted that, according to the NuDat3.0 database [40], the quadrupole deformation parameter (β_2) values for ^{120}Te is 0.121 while the reference data provided in TALYS lists the corresponding β_2 value of 0.197. The divergence in β_2 seems to have significantly impacted the theoretical cross-section calculations as evident in the two giant resonance peaks observed for S3, S7, and S10 combined with various LD models, resulting in subtantial discrepancies with the experimental values.

The combination of all six LD models with each specific γSF except for GD1M HFB + QRPA [S8] and SMLO [S9] γSFs display relatively comparable GDR cross-section behavior but demonstrate distinct variations at energies of 18 MeV and above. The HFB [S4] and GT-HFB [S6] γSFs exhibit fundamental similarities. Both are derived using the Hartree-Fock-Bogoliubov model built upon the Skyrme force with QRPA calculations. However, for S6, Goriely et al. [39] introduced an extension by incorporating a temperature-dependent term to the GDR width. Despite this modification, Figs. 2−5 clearly demonstrate that the GDR shapes for these two cases are identical. The calculated results of GD1M HFB + QRPA [S8] with GSM [LD3] express the best similarity with experimental data within the energy region of 12−20 MeV. There are still large discrepancies between theories and experiments especially for the tail of the resonance peak.

Entirely analogous to the previous reaction, in Fig. 3, γSFs HF-BCS [S3], T-RMF [S7], S-HFB + QRPA [S10] combined with different LD models, predict the cross-section of ^{122}Te (γ, n)^{121}Te reaction with two maxima, while the other γSFs exhibit only a single resonance peak. Except for cases where level density models are combined with GD1M HFB + QRPA [S8] or SMLO [S9], six level density models yield consistent cross-section predictions in the energy range from 10 to 18 MeV; beyond this range, the LDs show discrepancies. Following to NuDat3.0 database [40], the β_2 value of ^{122}Te is 0.131 whilst that in TALYS is 0.188, leading to the prediction of two GDR peaks resulted from the combinations of S3, S7 and S10 with different LD models. Unfortunately, no experimental findings are present in the existing literature. Therefore, future measurements are essential to validate the accuracy of the theoretical LD and γSF models for this case.

For the ^{128}Te(γ, n)^{127}Te reaction data demonstrated in Fig. 4, the agreements between theories and experiments seem reasonable. Particularly, the experimetal data of Lepretre [37] is nicely explained by the computed results of the phenomenological γSF model BAL [S2] and microscopic one S-HFB + QRPA [S10] with different LD models around the peak region ranging from 10 to 16 MeV. On the right side of GDR region, it reveals inconsistencies in all LD models.

In Fig. 5, for ^{130}Te(γ, n)^{129}Te reaction, analogy to the previous case, the GDR region is characterized by one peak and all combinations of LD and γSF predict relatively well the measured data taken from Ref. [37]. In the TALYS code, the β_2 values for ^{128}Te and ^{130}Te are 0.115, and 0.09, respectively which show slight discrepancies compared to the corresponding β_2 of 0.1352, and 0.1184 in the NuDat3.0 database. It is entirely reasonable that a nucleus with a small quadrupole deformation parameter, or in other words, a nearly spherical nucleus, exhibits only a single giant resonance peak. The combination of SHFB [LD4] or TGHFBC [LD6] with SHFB + QRPA [S10] provides the best agreement with the experimental values. Notably, the merger of LD4/LD6 model with other γSF produces higher results compared to other combinations in the right-hand region of the GDR. Similar to other reactions, the calculations for HFB [S4] yield outcomes identical to those for GT-HFB [S6]. However, the GDR peak height for the S4/S6 calculations underestimates the experimental data.

Comparing with experimental data to the right of the resonance peak allows for evaluating which level density theory is more accurate. However, this assessment remains challenging owing to the significant errors present in the experimental measurements in this region. This highlights the importance of comparing theory with experiment based on IRs rather than cross sections. This comparison will be further discussed in the following subsection of this paper.

Futhermore, the cross sections for producing ^{119}Te, ^{121}Te, ^{127}Te and ^{129}Te isotopes at the isomeric and ground states through (γ, n) reactions using

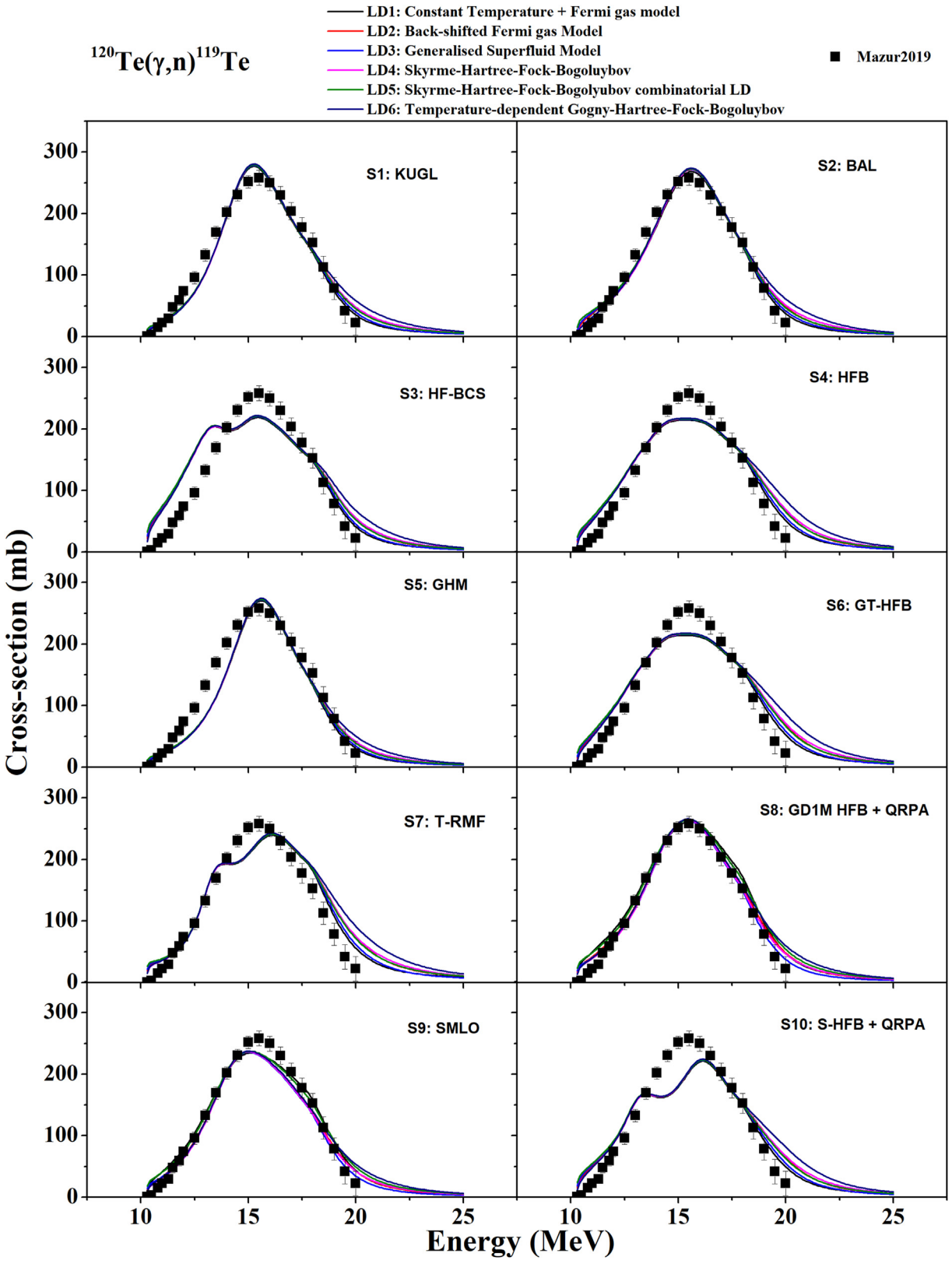

Fig. 2. The calculated cross-sections of $^{120}Te(\gamma, n)^{119}Te$ reaction using different combinations of existing LD and γSF in TALYS 2.0 along with experimental values [36].

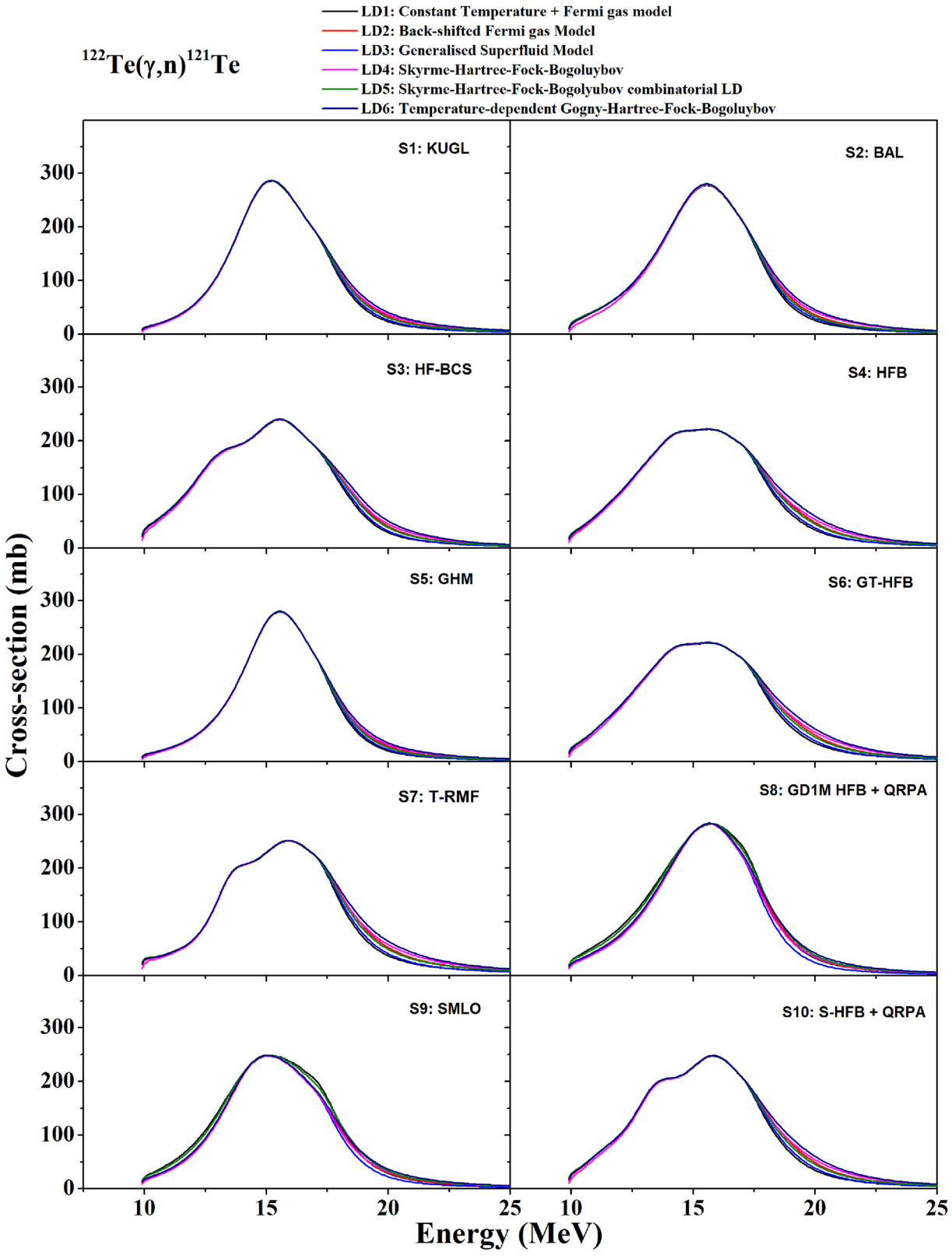

Fig. 3. The calculated cross-sections of ^{122}Te (γ, n)^{121}Te reaction using different combinations of existing LD and γSF in TALYS 2.0.

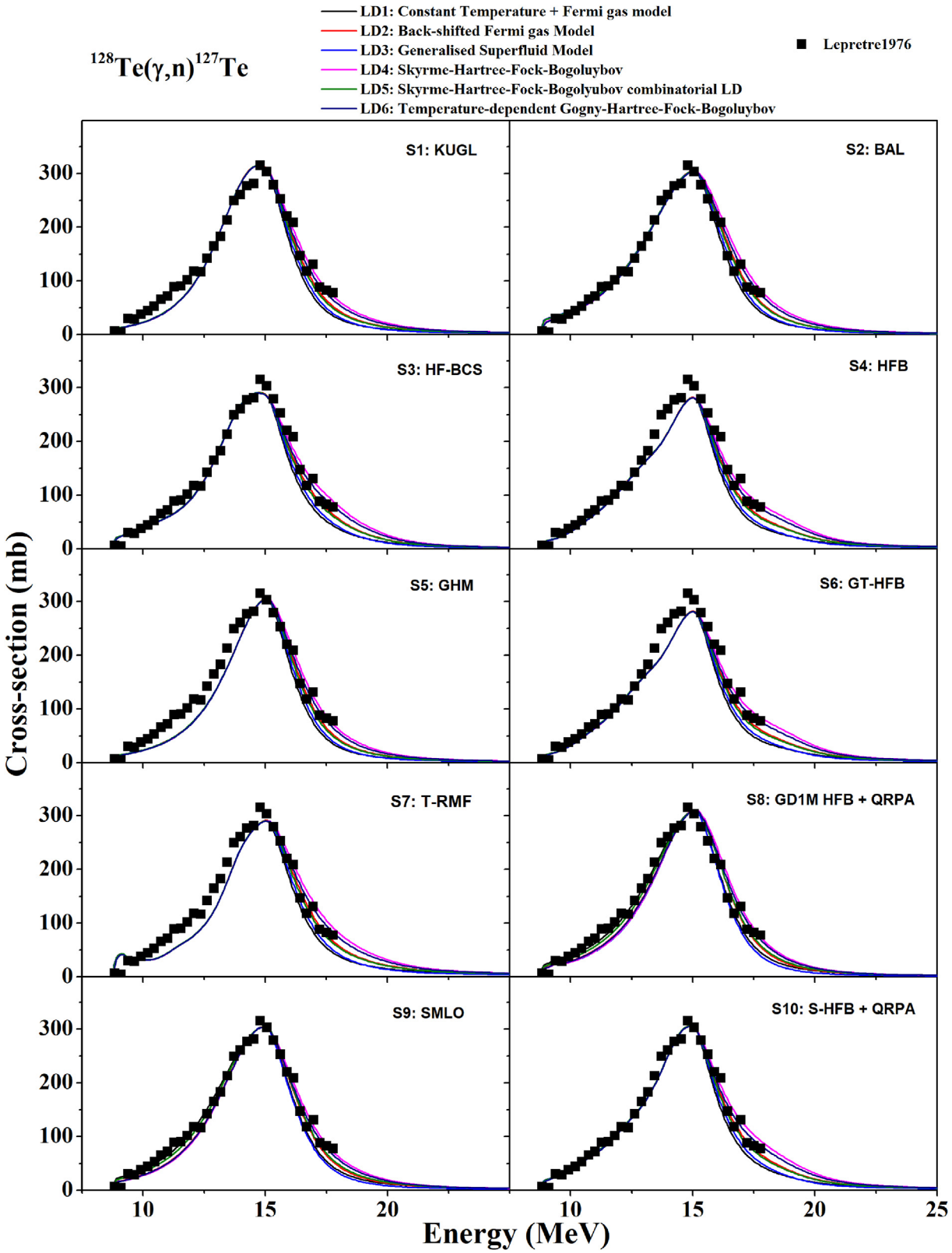

Fig. 4. The calculated cross-sections of ^{128}Te (γ, n)^{127}Te reaction using different combinations of existing LD and γSF in TALYS 2.0 along with experimental values [37].

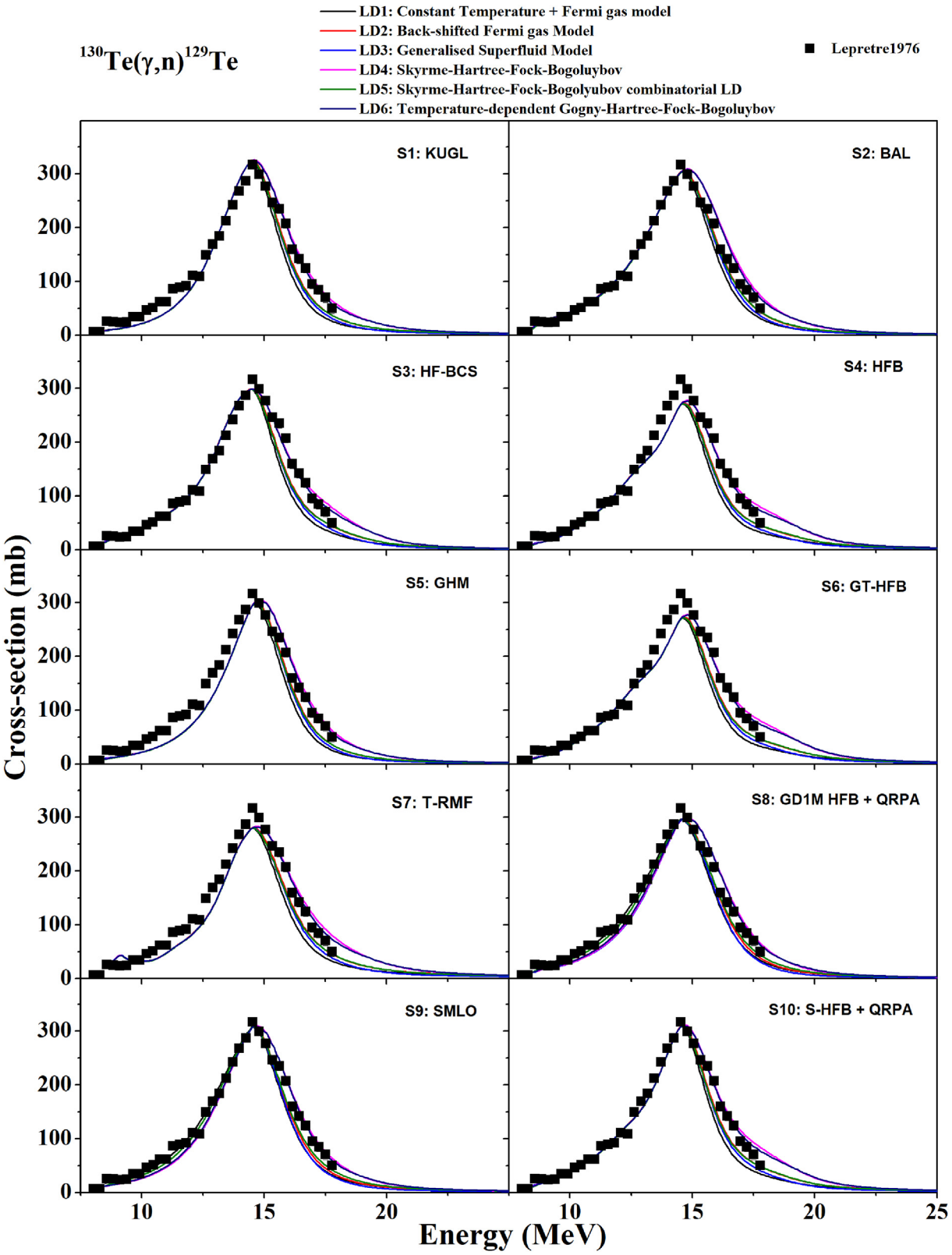

Fig. 5. The calculated cross sections of ^{130}Te (γ, n)^{129}Te reaction using different combinations of existing LD and γSF in TALYS 2.0 along with experimental values [37].

combinations of six LD models and γSF SMLO [S9] in TALYS 2.0 code are depicted in Fig. 6.

It can be observed that, although total cross-sections are nearly identical except for the right-hand region of the GDR peak, as shown in Figs. 2−5, there are significant disagreement among the LD models used for calculating the isomeric production cross-sections, while the differences are relatively smaller for that of

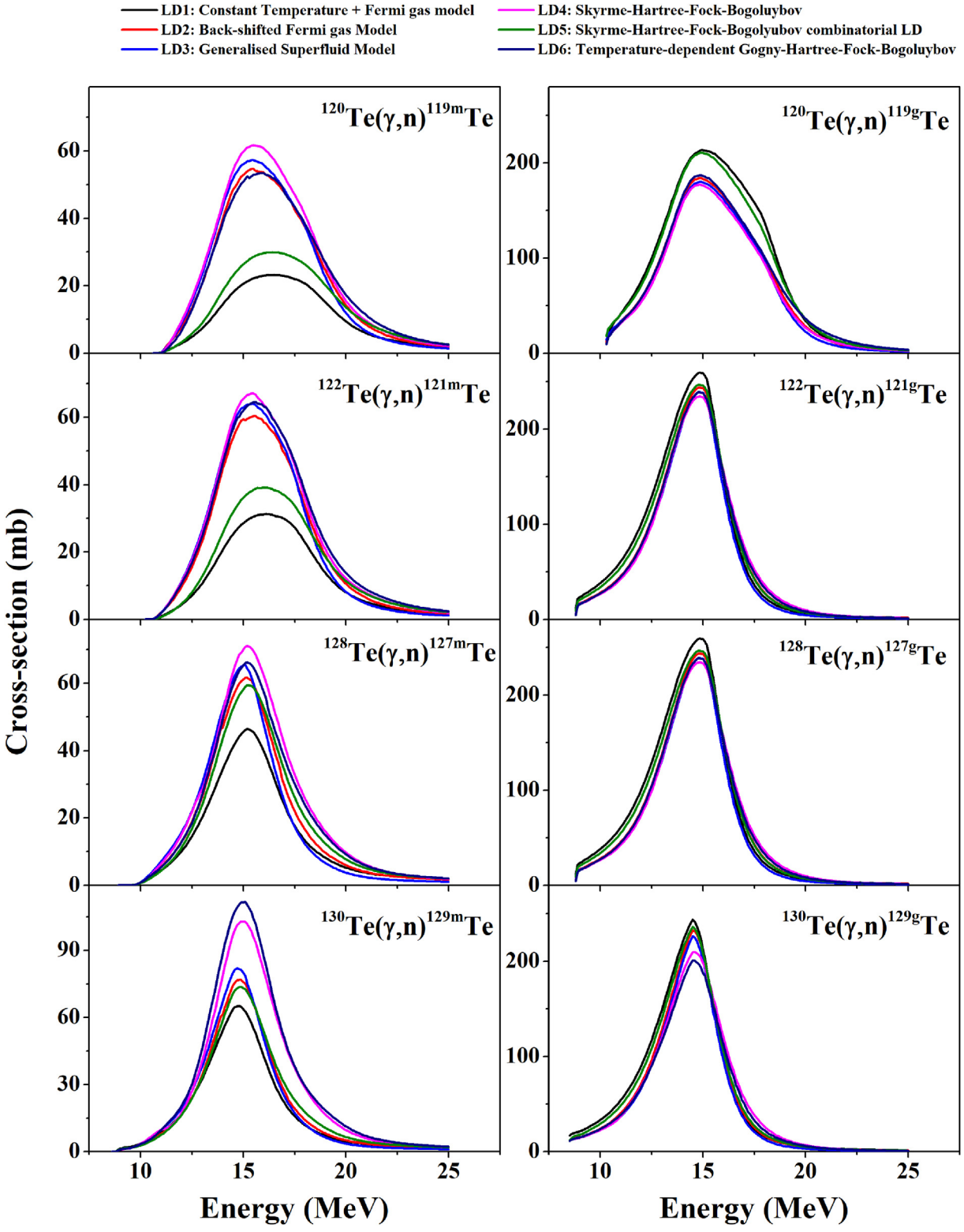

Fig. 6. The cross-sections for producing isomeric pairs of ^{119,121,127,129}Te through (γ, n) reactions using combinations of six LD models and SMLO [S9] in TALYS 2.0 code.

the ground state. This deviation may arise from variations in spin distribution among the LD models.

Fig. 7 illustrates the calculated contributions of compound, pre-equilibrium, and direct processes to the total photoneutron reaction cross-section on isotopes ^{119,121,127,129}Te, using the SHFB [LD4] and KUGL [S1] models as a representative example.

The calculations indicate that compound mechanisms dominate in the GDR region, with their contribution to the total (γ, n) cross sections exceeding 90 %, while the pre-equilibrium contribution is minimal, and the direct process is completely absent.

3.3. Isomeric ratio

The calculated IRs were derived from the convolution of TALYS-based calculated differential cross-sections with GEANT4-based simulated bremsstrahlung spectra. Detailed comparisons between the calculated theoretical IRs and experimental values for isomeric pairs ^{119m,g}Te, ^{121m,g}Te, ^{127m,g}Te and ^{129m,g}Te are presented in Figs. 8−11. Attention is drawn to the fact that the computed results exhibit significant variations in IRs depending on the choice of LD models and γSFs, highlighting the critical influence of these factors in the calculations.

A consistent trend in the dependence of the IR on bremsstrahlung end-point energies in the range of 10−25 MeV was identified in both theoretical predictions and experimental data for the isomeric pairs ^{119m,g}Te, ^{121m,g}Te, ^{127m,g}Te and ^{129m,g}Te. The IRs exhibit a rapid increase from the reaction threshold to the peak of the GDR region, followed by a more gradual rise. This behavior is reasonable, as the transfer of angular momentum to the compound nucleus at low energies contributes to a significant increase in IR alongside rising excitation energy. At higher energies, the IR continues to grow moderately, likely influenced by the contributions of pre-equilibrium and direct reaction mechanisms, as well as other competing channels.

Additionally, the theoretical results indicate that the IR increases with the enhancement of isotope mass from A = 119 to A = 129. This phenomenon is also corroborated by experimental data reported in Refs.

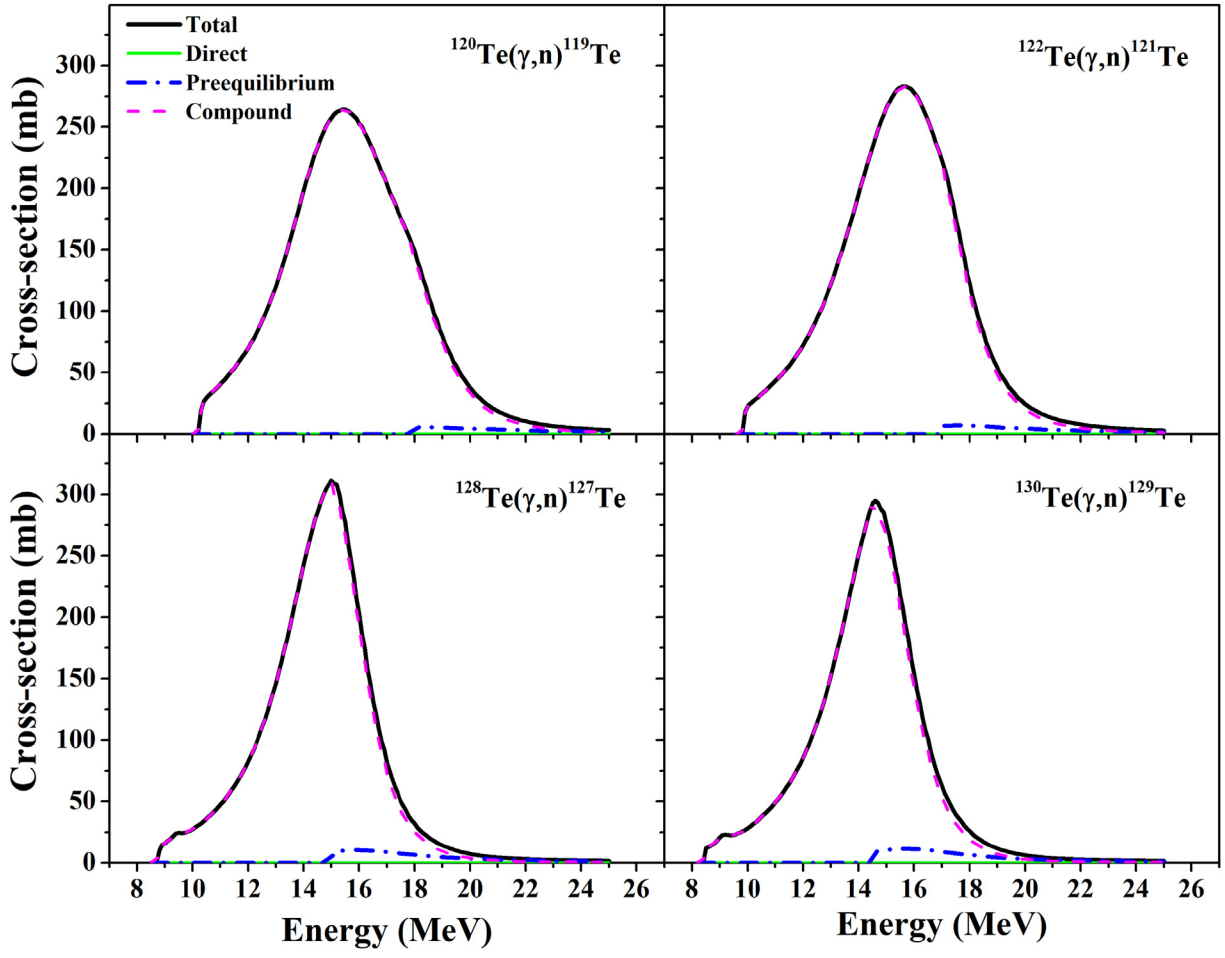

Fig. 7. Cross-sections for the (γ, n) reaction on ^{120,122,128,130}Te nuclei.

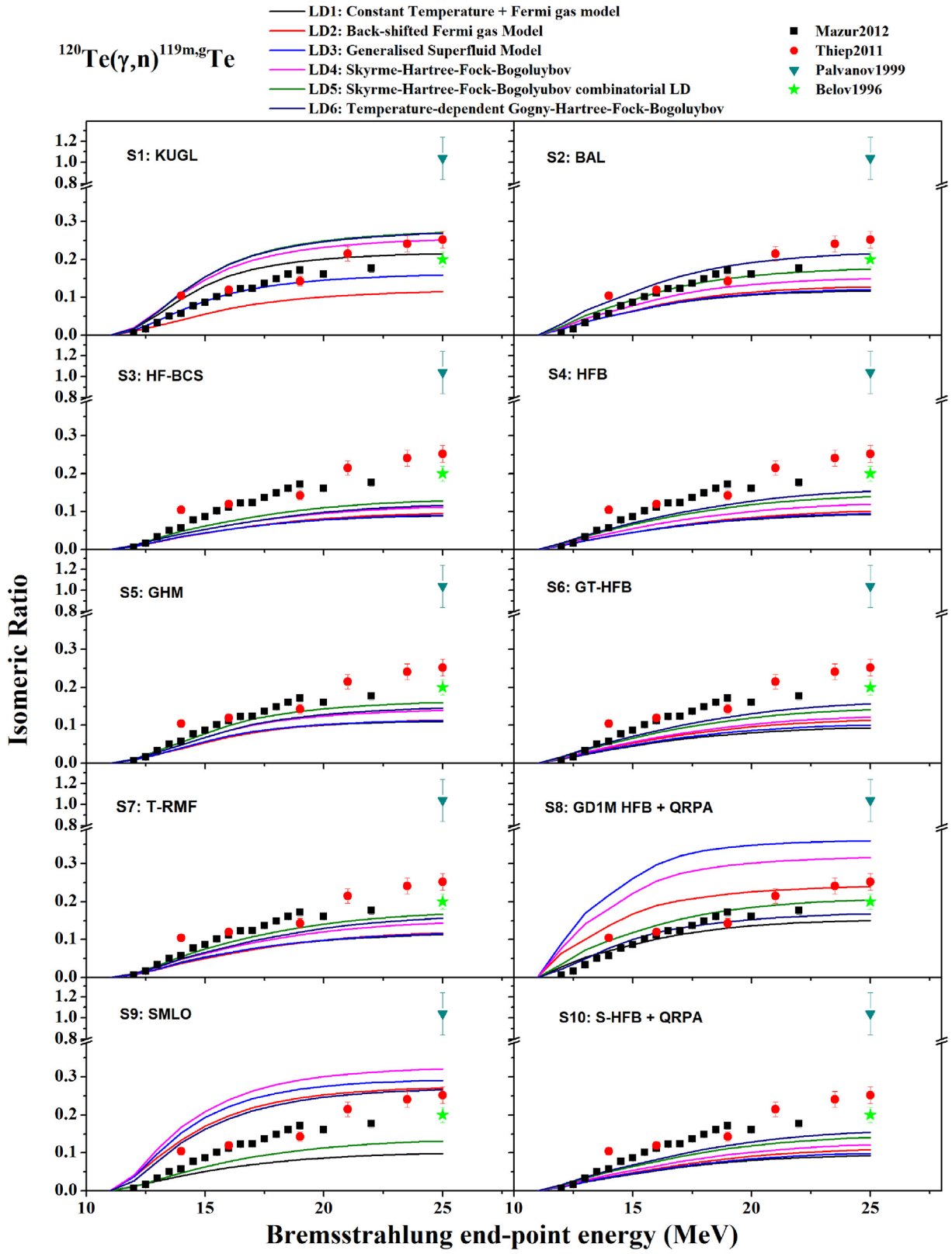

Fig. 8. The calculated IRs of ^{119m,g}Te using different combinations of existing LD and γSF in TALYS 2.0 in comparison with the literature.

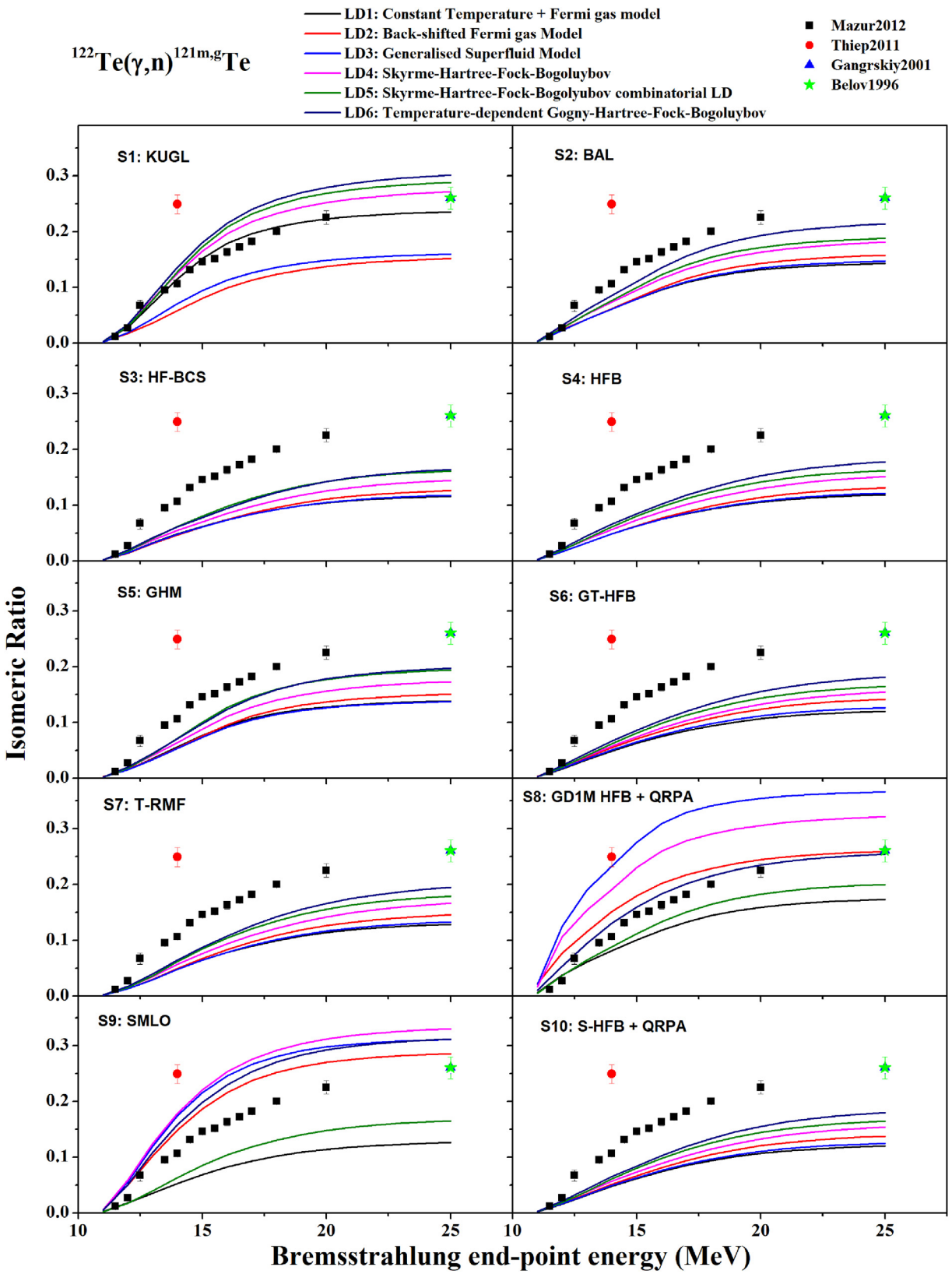

Fig. 9. Theoretically calculated IRs of ^{121m,g}Te using different combinations of existing LD and γSF in TALYS 2.0 in comparison with the literature.

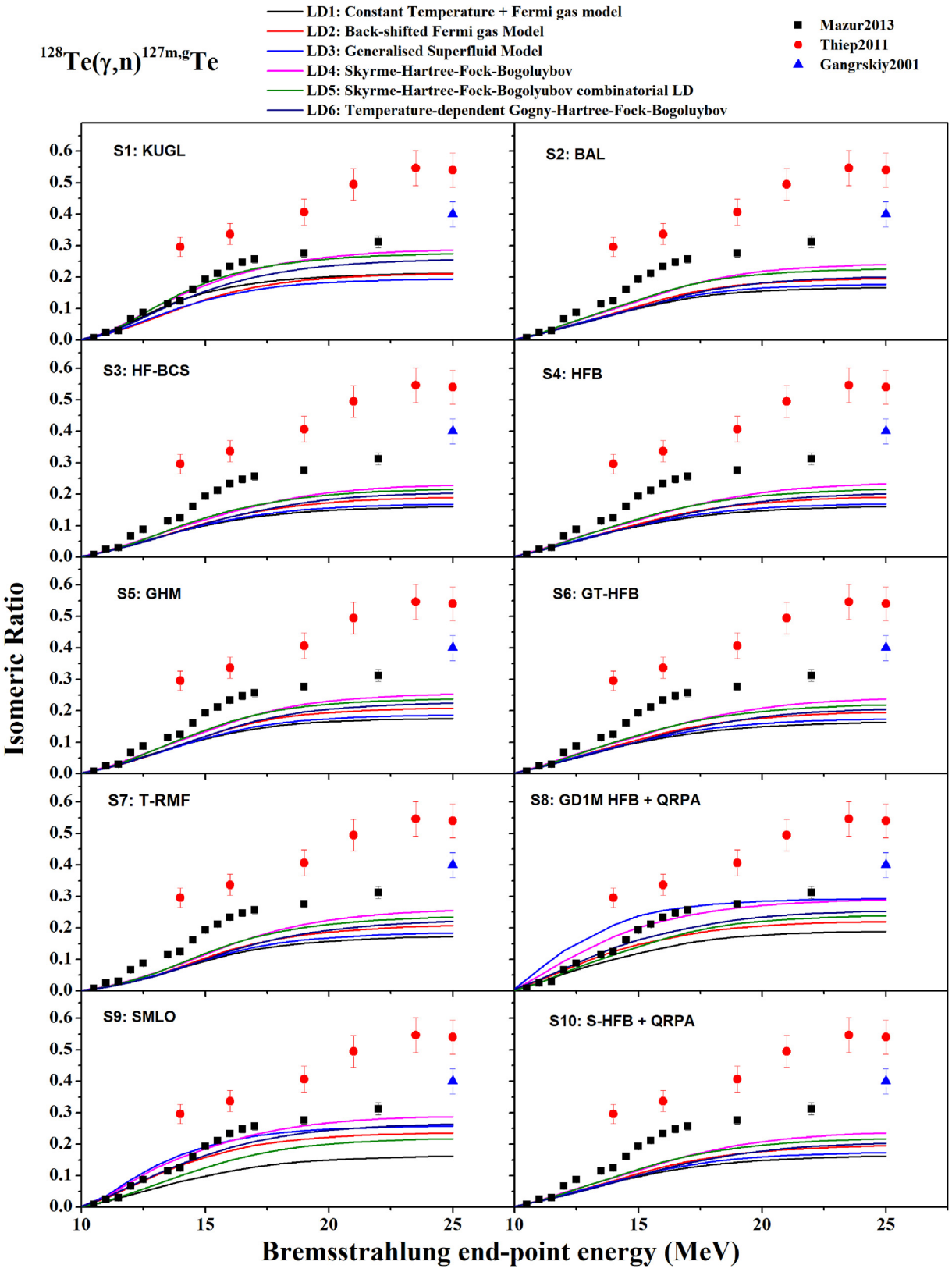

Fig. 10. Theoretically calculated IRs of ^{127m,g}Te using different combinations of existing LD and γSF in TALYS 2.0 in comparison with the literature.

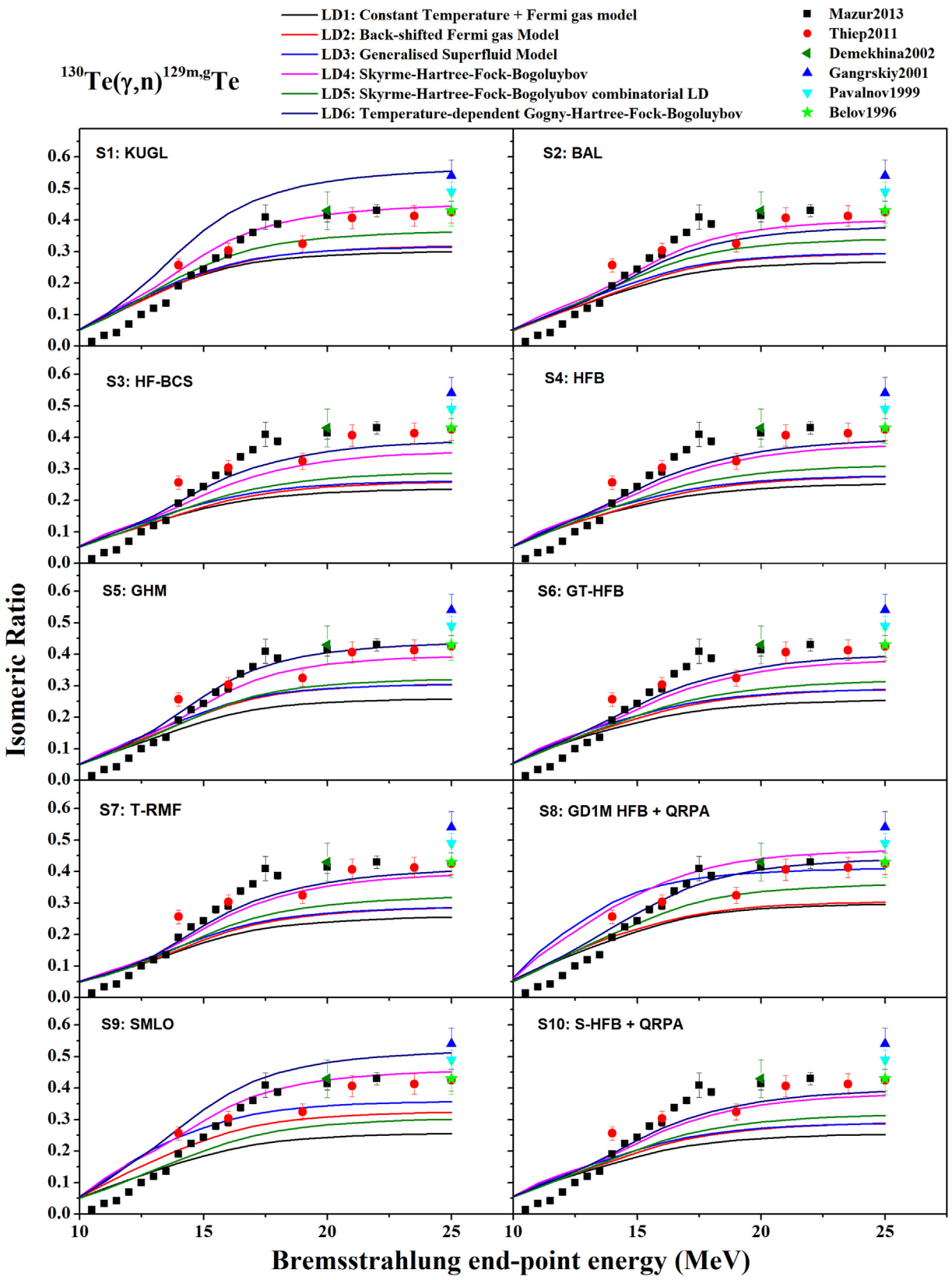

Fig. 11. Theoretically calculated IRs of ^{129m,g}Te using different combinations of existing LD and γSF in TALYS 2.0 in comparison with the literature.

[16,17,19,20], although it is not observed in Refs. [10,18]. Another effect is observed in both theoretical values and experimental data concerning the spin of isomeric pairs. The spin of isomers ^{119m}Te, ^{121m}Te, ^{127m}Te and ^{129m}Te is 11/2-, while the ground state spin is 1/2+ for ^{119g}Te and ^{121g}Te, and 3/2+ for ^{127g}Te and ^{129g}Te. The results reveal that IRs of ^{127mg}Te and ^{129mg}Te are higher than that of ^{119m,g}Te and ^{121m,g}Te, namely, IR increases with the rise in the ground state spin.

Fig. 8 illustrates the calculated IRs of ^{119m,g}Te obtained using various combinations of available LD and γSF models in TALYS 2.0, compared with values reported in the EXFOR library.

The trend in experimental data for IRs of ^{119m,g}Te from previous studies shows significant inconsistency in the energy range from 19 MeV and above. However, it is evident that the results obtained by using KUGL [S1], BAL [S2], and GD1M HFB + QRPA [S8] γSFs align best with the experimental data. The SMLO [S9] combining with CT + FG [LD1] or SHFBC [LD5] (S9 + LD1/LD5) underpredict the experimental data while S9 with the other LD models overpredict the experimental data. The remaining γSFs with different LD models underpredict the exprimental data. Only a handful of LD models for each of the S1, S2, and S8 γSFs match the experimental results, underscoring the importance of this study in ruling out less accurate theories. Specifically, the calculated values using S1 + LD3, S2 + LD5 or S8 + LD6 expresses a good similarity with the experimental data in Ref. [16] and the values in Ref. [10] at 16 and 19 MeV, whereas the data at 14, 23.5 and 25 MeV in Ref. [10] are nicely explained by the results of S1 + LD4 calculations.

The IRs of ^{121m,g}Te, calculated using various LD and γSF model combinations in TALYS 2.0, are shown in Fig. 9, with comparisons to literature values. In the case of ^{121m,g}Te, the experimental data points exhibit significant discrepancies, which may be related to uncertainties in estimating systematic errors and the half-life. Notably, in the case of ^{121}Te and ^{127}Te, there is a relative mismatch between the results reported by Refs. [10,16], attributed to differences in the half-life values referenced in different databases. In Thiep's study, the half-lives of the Te isotopes were taken from Ref. [41], whereas Mazur's study referred to the *Nuclear Data Sheets* [42,43]. The half-lives for ^{121m}Te, ^{121g}Te, and ^{127m}Te were reported as 154 days, 16.8 days, and 109.0 days, respectively, in Thiep's work, compared to 164.2 days, 19.17 days, and 106.1 days in Mazur's. It can be observed that the computed outcome using the S8 + LD3 model is in good agreement with the experimental value of [10], while S1 + LD1 align well with the remaining three experimental sets [16,19,20].

Fig. 10 presents the IRs of ^{127m,g}Te calculated using different LD and γSF model combinations in TALYS 2.0, alongside comparisons with previously published data.

The case of ^{127m,g}Te is analogous to that of ^{121m,g}Te; however, it exhibits a greater number of red experimental data points [10] compared to the former case, along with systematically higher values. This discrepancy may be attributed to an error in the systematic uncertainty assessment in one of the experiments and the differing half-life references, as previously discussed. In this scenario, most γSFs, with the exception of GD1M HFB + QRPA [S8], produce results lower than the experimental data. The experimental results reported by Mazur [17] are consistent with the theoretical predictions derived from the S8 + LD6 or S9 + LD2/LD6 combinations in the energy range of 10−13.5 MeV, whereas at higher energies, the S8 + LD4 model calculations exhibit a slight correlation.

Fig. 11 depicts the IRs of ^{129mg}Te calculated using different LD and γSF model combinations in TALYS 2.0, compared to previously published findings.

For the case of ^{129m,g}Te, the experimental data points are in good agreement with each other and also show a consistent trend. However, when compared with theoretical predictions, it becomes clear that most increasing trends in the IR do not align with the experimental data. This highlights a significant issue with the theory applied in this case, calling for improved theoretical models. It is particularly noteworthy that between 10 and 13.5 MeV, all theoretical results overpredict the experimental values. In the higher energy region, calculations employing the SHFB [LD4] model combined with KUGL [S1] or SMLO [S9], and TGHFBC [LD6] paired with GHM [S5] or GD1M HFB + QRPA [S8], demonstrate a moderate alignment with the experimental data.

4. Conclusions

The IRs of four isomeric pairs ^{119mg}Te, ^{121mg}Te, ^{127mg}Te and ^{129mg}Te produced in bremsstrahlung-irradiated reactions within the GDR region have been computed by employing a combination of the TALYS 2.0 code and the GEANT4 toolkit. The combinations of six LD models and ten γSFs available in TALYS 2.0 have been implemented to survey the influence of different LD and γSF models on the cross-sections and IRs of Te isotopes. The calculated results were compared with the experimetal data in EXFOR library to verify the reliability of the theoretical models. The calculations demonstrated a distinct trend in the dependence of IR on bremsstrahlung end-point energies for the isomeric pairs ^{119m,g}Te, ^{121m,g}Te, ^{127m,g}Te and ^{129m,g}Te. Furthermore, the results highlighted that the

compound reaction mechanism predominates within the GDR region, underscoring its critical role in the observed behavior. The effects of the excitation energy, isotope mass dependence, and spin on the IRs were also investigated. This confirms the reliability of GEANT4 and TALYS codes as robust tools for estimating cross-sections and IRs of Te isotopes in photonuclear reactions within the GDR region. The calculations reveal notable variations in cross-section and IRs arising from the selection of LD models and γSFs, reflecting the critical impact of these parameters on the accuracy of describing and predicting photonuclear reaction cross-sections and IRs for Te isotopes. The deficiencies of nuclear models with inaccurate descriptions should be addressed and improved in future studies.

Funding

This work was financially supported by the Institute of Physics, Vietnam Academy of Science and Technology, Vietnam under the 2024 funding program for young scientists, through the project titled: *"Calculation and Evaluation of Several Characteristics of Photonuclear Reactions Induced by Bremsstrahlung*".

Conflict of interest

The authors declare no conflicts of interest.

References

[1] A. Zilges, et al., Photonuclear reactions—from basic research to applications, Prog. Part. Nucl. Phys. 122 (2022) 103903.
[2] T. Rauscher, Photonuclear reactions in astrophysics, Nucl. Phys. News 28 (3) (2018) 12−15.
[3] H. Naik, et al., Measurement of the flux-weighted cross-sections for the ^{nat}Yb (γ, xn) ^{175,169,167}Yb reactions in the Bremsstrahlung end-point energies of 12−16 MeV and 60−70 MeV, European Phys. J. A 59 (10) (2023) 249.
[4] Nguyen Van Do, et al., Measurement of the integrated cross section of ^{110}Pd (γ, n) ^{109m}Pd, ^{110}Pd (γ, n) ^{109g}Pd, and ^{110}Pd (γ, x) ^{108m}Rh reactions with 70 MeV bremsstrahlung, Radiat. Phys. Chem. 203 (2023) 110598.
[5] Nadeem Muhammad, et al., Measurements of ^{nat}Cd (γ, x) reaction cross sections and isomer ratio of ^{115m,g}Cd with the bremsstrahlung end-point energies of 50 and 60 MeV, Chin. Phys. C 45 (12) (2021) 124002.
[6] Thiep Tran Duc, et al., The isomeric ratios in some photonuclear reactions (γ, n), (γ, p), (γ, 2n), and (γ, np) induced by bremsstrahlungs with end-point energies in the Giant Dipole Resonance region, Phys. Part. Nuclei. Lett. 6 (2009) 126−133.
[7] Thiep Tran Duc, et al., Channel effect in isomeric ratio of ^{137m,g}Ce produced in different nuclear reactions, J. Radioanal. Nucl. Chem. 314 (2017) 1777−1784.
[8] Tran Duc Thiep, et al., Isomeric yield ratios of ^{195m,g}Hg and ^{197m,g}Hg in the ^{196}Hg (γ, n) and ^{198}Hg (γ, n) reactions induced by bremsstrahlung energy within giant dipole resonance region, Nucl. Instrum. Methods Phys. Res. Sect. B Beam Interact. Mater. Atoms 457 (2019) 4−9.
[9] Thiep Tran Duc, et al., Isomeric ratio of ^{137m}Ce to ^{137g}Ce produced in ^{138}Ce(γ, n) ^{137m,g}Ce photonuclear reaction induced by end-point bremsstrahlung energies from 14 to 17, 21 to 23 and at 19 MeV, J. Radioanal. Nucl. Chem. 311 (2017) 887−892.
[10] Thiep Tran Duc, et al., The isomeric ratios in photonuclear reactions of natural tellurium induced by bremsstrahlungs with endpoint energies in the giant dipole resonance region, J. Radioanal. Nucl. Chem. 289 (2011) 637−645.
[11] Thiep Tran Duc, et al., The isomeric ratios in photonuclear reactions of natural barium induced by bremsstrahlung with endpoint energies in the giant dipole resonance region, J. Radioanal. Nucl. Chem. 292 (1) (2012) 89−96.
[12] B.M. Hue, T.D. Thiep, T.T. An, P.V. Cuong, S.M. Lukyanov, S. Mitrofanov, Isomeric ratios in neutron capture reaction, induced by thermal, resonant and mixed thermal-resonant neutrons on ^{114}Cd and ^{116}Cd nuclei, Nucl. Instrum. Methods Phys. Res. Sect. B Beam Interact. Mater. Atoms 502 (2021) 46−53.
[13] J.R. Huizenga, Rt Vandenbosch, Interpretation of isomeric cross-section ratios for (n, γ) and (γ, n) reactions, Phys. Rev. 120.4 (1960) 1305.
[14] R. Vandenbosch, J.R. Huizenga, Isomeric cross-section ratios for reactions producing the isomeric pair Hg^{197,197m}, Phys. Rev. 120 (4) (1960) 1313.
[15] N.A. Demekhina, A.S. Danagulyan, G.S. Karapetyan, Analysis of isomeric ratios in (γ, n) and (γ, p) reactions around giant-resonance energies, Phys. Atom Nucl. 65 (2002) 365−370.
[16] V.M. Mazur, et al., Cross-sections of isomeric state excitation of the 119 Te and 121 Te nuclei in (γ, n) reactions in an energy range of 9−20 MeV, Phys. Part. Nuclei. Lett. 9 (2012) 248−252.
[17] V.M. Mazur, et al., Excitation of the ^{119m}Te, ^{121m}Te, ^{123m}Te, ^{127m}Te, and ^{129m}Te isomers in (γ, n) reactions from 10 to 22 MeV, Phys. Rev. C: Nucl. Phys. 87 (4) (2013) 044604.
[18] S.R. Palvanov, O. Razhabov, Isomer yield ratios of photonuclear reactions at E γmax 25 and 30 MeV, Atom. Energy 87 (1) (1999) 533−536.
[19] Yu.P. Gangrskiy, Isomeric ratios in crossing (n, γ) and (γ, n) reactions, Bull. Russ. Acad. Sci. Phys. 65 (Issue.1) (2001) 121.
[20] A.G. Belov, et al., Excitation of isomeric $1h_{11/2}$ states in the reactions (γ, n), Phys. Atom Nucl. 59 (4) (1996) 553−559.
[21] P.G. Young, E.D. Arthur, M.B. Chadwick, The GNASH nuclear model code, in: M.K. Mehta, J.J. Schmidt (Eds.), Workshop on Computation and Analysis of Nuclear Data Relevant to Nuclear Energy and Safety, 1993, p. 622. Feb. 10 - March 13 1992, Trieste, Italy.
[22] M. Blann, Recent progress and current status of pre-equilibrium reaction theories and computer code ALICE, in: M.K. Mehta, J.J. Schmidt (Eds.), Workshop on Computation and Analysis of Nuclear Data Relevant to Nuclear Energy and Safety, 1993, p. 622. Feb. 10 - March 13 1992, Trieste, Italy.
[23] M. Uhl, B. Strohmaier, Computer Code for Particle Induced Activation Cross Sections and Related Quantities, 1976. *IRK Vienna report* 76/01.
[24] M. Herman, et al., EMPIRE: nuclear reaction model code system for data evaluation, Nucl. Data Sheets 108 (2007) 2655.
[25] Arjan Koning, Stephane Hilaire, Stephane Goriely, TALYS: modeling of nuclear reactions, The European Physical Journal A 59 (6) (2023) 131.
[26] TALYS-2.0, A.J. Koning, S. Hilaire, S. Goriely, TALYS User Manual - A Nuclear Reaction Program, NRG-1755 ZG PETTEN, Netherlands, 2023.
[27] P.V. Cuong, T.D. Thiep, L.T. Anh, T.T. An, B.M. Hue, K.T. Thanh, N.H. Tan, N.T. Vinh, T.T. Anh, Theoretical calculation by Talys code in combination with Geant4 simulation for consideration of (γ, n) reactions of Eu isotopes in the giant dipole resonance region, Nucl. Inst. Methods Phys. Res. B 479 (2020) 68−73.
[28] Minh Hue Bui, Duc Thiep Tran, Theoretical consideration of isomeric ratios in some photonuclear reactions induced by bremsstrahlung with endpoint energy in giant dipole resonance region using Talys 1.95 code, Nucl. Sci. Technol. 12 (1) (2022) 21−31.
[29] Agostinelli Sea, et al., GEANT4—a simulation toolkit, Nucl. Inst. Methods Phys. Res. A 506 (3) (2003) 250−303.
[30] R. Arthur Forster, et al., "MCNP version 5". Nuclear instruments and methods in physics research section B: beam interactions

with materials and atoms, in: 5th Topical Meeting on Industrial Radiation and Radioisotope Measurement Applications, 213, 2004, pp. 82−86, issn: 0168-583X.
[31] Giuseppe Battistoni, et al., Overview of the FLUKA code, Ann. Nucl. Energy 82 (2015) 10−18.
[32] Paweł Bzowski, et al., Efficiency of 124I radioisotope production from natural and enriched tellurium dioxide using 124Te (p, xn) 124I reaction, EJNMMI Phys. 9 (1) (2022) 41.
[33] Robbie Haffner, William H. Miller, Steve Morris, Verification of I-131 Yields from the neutron irradiation of tellurium, Appl Radiat Isot 151 (2019) 52−61.
[34] Trevor Ferris, et al., Use of radioiodine in nuclear medicine—a brief overview, J. Label Compd. Radiopharm. 64 (3) (2021) 92−108.
[35] V.V. Zerkin, B. Pritychenko, The experimental nuclear reaction data (EXFOR): extended computer database and Web retrieval system, Nucl. Inst. Methods Phys. Res. A 888 (2018) 31−43.
[36] V.M. Mazur, et al., Study of the cross sections for (γ, n)-reactions on p-nuclei 120 Te, 136 Ce in the giant E1-resonance energy region, Yaderna Fyizika ta Energetika 20 (3) (2019) 228−234.
[37] A. Leprêtre, et al., A study of the giant dipole resonance in doubly even tellurium and cerium isotopes, Nucl. Phys. 258 (2) (1976) 350−364.
[38] Rene Brun, Fons Rademakers, ROOT—an object oriented data analysis framework, Nucl. Instrum. Methods Phys. Res. Sect. A Accel. Spectrom. Detect. Assoc. Equip. 389 (1−2) (1997) 81−86.
[39] S. Goriely, E. Khan, M. Samyn, Microscopic HFB + QRPA predictions of dipole strength for astrophysics applications, Nucl. Phys. A 739 (3) (2004) 331−352.
[40] NuDat 3.0, National Nuclear Data Center, Brookhaven National Laboratory, Available at: https://www.nndc.bnl.gov/nudat3/.
[41] Richard B. Firestone, Virginia S. Shirley, Table of Isotopes, 1998, 2 volume set.
[42] S. Ohya, Nucl. Data Sheets 111 (2010) 1619.
[43] A. Hashizume, Nucl. Data Sheets 112 (2011) 1647.